



Title	Prediction of the treatment outcome using intravoxel incoherent motion and diffusional kurtosis imaging in nasal or sinonasal squamous cell carcinoma patients
Author(s)	Fujima, Noriyuki; Yoshida, Daisuke; Sakashita, Tomohiro; Homma, Akihiro; Tsukahara, Akiko; Shimizu, Yukie; Tha, Khin Khin; Kudo, Kohsuke; Shirato, Hiroki
Citation	European radiology, 27(3), 956-965 https://doi.org/10.1007/s00330-016-4440-1
Issue Date	2017-03
Doc URL	http://hdl.handle.net/2115/68399
Rights	The original publication is available at www.springerlink.com
Type	article (author version)
File Information	EurRadiol27_956.pdf



[Instructions for use](#)

ORIGINAL RESEARCH

Prediction of the Treatment Outcome Using Intravoxel Incoherent Motion and Diffusional Kurtosis Imaging in Nasal or Sinonasal Squamous Cell Carcinoma Patients

Noriyuki Fujima, MD, PhD¹; Daisuke Yoshida, MD¹; Tomohiro Sakashita, MD, PhD²;
Akihiro Homma, MD, PhD²; Akiko Tsukahara, MD¹; Yukie Shimizu, MD¹; Khin Khin
Tha, MD, PhD^{3,4}; Kohsuke Kudo, MD, PhD¹; and Hiroki Shirato, MD, PhD^{3,4}

¹ Department of Diagnostic and Interventional Radiology, Hokkaido University Hospital

² Department of Otolaryngology-Head and Neck Surgery, Hokkaido University
Graduate School of Medicine

³ Department of Radiation Medicine, Hokkaido University Graduate School of
Medicine

⁴ The Global Station for Quantum Medical Science and Engineering, Global Institution
for collaborative research and education

Corresponding Author

Noriyuki Fujima

Department of Diagnostic and Interventional Radiology, Hokkaido University Hospital

N15, W7, Kita-Ku, Sapporo 060-8638, Japan

Phone: +81-11-706-5977; Fax: +81-11-706-7876

E-mail: Noriyuki.Fujima@mb9.seikyuu.ne.jp

Funding information

This study has received grant support from Ministry of Education, Culture, Sports,

Science and Technology – Japan (ID; 25861047)

Manuscript title

Prediction of the Treatment Outcome Using Intravoxel Incoherent Motion and
Diffusional Kurtosis Imaging in Nasal or Sinonasal Squamous Cell Carcinoma Patients

Manuscript type

Original Research

ABSTRACT

Objectives: To evaluate the diagnostic value of intravoxel incoherent motion (IVIM) and diffusional kurtosis imaging (DKI) parameters in nasal or sinonasal squamous cell carcinoma (SCC) patients to determine local control/failure.

Methods: Twenty-eight patients were evaluated. MR acquisition used single-shot spin-echo EPI with 12 b-values. Quantitative parameters (mean value, 25th, 50th and 75th percentiles) of IVIM (perfusion fraction f , pseudo-diffusion coefficient D^* , and true-diffusion coefficient D), DKI (kurtosis value K , kurtosis corrected diffusion coefficient D_k) and apparent diffusion coefficient (ADC) were calculated. Parameter values at both the pretreatment and early-treatment period, and the percentage change between these two periods were obtained.

Results: Multivariate logistic regression analysis: the percentage changes of D (mean, 25th, 50th, 75th), K (mean, 50th, 75th), D_k (mean, 25th, 50th), and ADC (mean, 25th, 50th) were predictors of local control. ROC curve analysis: the parameter with the highest accuracy = the percentage change of D value with the histogram 25th percentile (0.93 diagnostic accuracy). Multivariate Cox regression analyses: the percentage changes of D (mean, 25th, 50th), K (mean, 50th, 75th), D_k (mean, 25th, 50th) and ADC (mean, 25th, 50th) are predictors.

Conclusions: IVIM and DKI parameters, especially the D-value's histogram 25th percentile, are useful for predicting local control.

Keywords

Magnetic resonance imaging

Squamous cell carcinoma of the head and neck

Diffusion Magnetic Resonance Imaging

Prognosis

Treatment Outcome

Key points

- Noninvasive assessment of treatment outcome in SCC patients was achieved using IVIM/DKI.
- Several IVIM and DKI parameters can predict the local control.
- Especially, the D-value's histogram 25th percentile has high diagnostic accuracy.

Abbreviations and acronyms

ADC; apparent diffusion coefficient

AUC; area under the curve

CI; confidence interval

DKI; diffusional kurtosis imaging

DWI; diffusion weighted imaging

EPI; echo-planar imaging

HR; hazard ratio

IVIM; intravoxel incoherent motion

MRI; magnetic resonance imaging

OR; odds ratio

RECIST; Response Evaluation Criteria in Solid Tumors

ROI; region of interest

SCC; squamous cell carcinoma

T1WI; T1 weighted image

T2WI; T2 weighted image

TSE; turbo spin-echo

INTRODUCTION

Surgical resection, chemotherapy, radiotherapy, and their combinations are common treatments for head and neck squamous cell carcinoma (SCC), including nasal or sinonasal cavity SCC [1]. Super-selective arterial infusions of cisplatin with concomitant radiotherapy, in particular, have become popular for SCC because of its higher local control rate in advanced cases of nasal or sinonasal SCC [2, 3]. For such a nonsurgical therapy, it would be helpful to be able to predict — either before treatment or during the early treatment period — the treatment results of patients who may fail to respond to treatment at the primary site; doing so could optimize patient management. Especially, arterial infusion therapy has great opportunity to optimize the treatment by adjusting distribution and dose of anticancer drug, compared to the systemic therapy.

For assessing treatment results, the Response Evaluation Criteria in Solid Tumors (RECIST) criteria provide a standard method [4], but it was reported that tumor size information is not very reliable for predicting treatment outcomes [5]. A 2012 review article contended that the tumor diffusion and perfusion reflects the tumor microenvironment and reveals its relation to treatment results [6]. The apparent diffusion coefficient (ADC) obtained by diffusion-weighted imaging (DWI)

noninvasively reveals the tumor microenvironment of tumor cellular density, and the ADC was useful for predicting patient prognoses [7, 8].

In recent years, extended models of DWI have been described for lesions in the head and neck [9-18] and also other organs such as lung [19]. In such extended models of DWI, intravoxel incoherent motion (IVIM) reveals more details about intratumoral diffusion than the ADC by using bi-exponential fitting with the division of the slow and fast diffusion components [20]. Fast and slow diffusion respectively reflect the tissue perfusion component and the extravascular component. Diffusional kurtosis imaging (DKI) reflects the non-Gaussian water diffusion and thus can provide a specific measure of tissue structure, such as cellular compartments and membranes [21]. IVIM and DKI can clarify the tumor microstructural condition and provide useful information to determine the treatment effect. There has been only a very limited amount of research investigating the utility of IVIM and DKI for elucidating treatment responses in SCC, and systematic studies of both IVIM and DKI in SCC patients are needed to predict treatment response.

Here we assessed the usefulness of IVIM and DKI parameters as a predictor of local control versus failure in nasal or sinonasal SCC patients.

MATERIALS AND METHODS

Subjects

Our institutional review board approved the study protocol. Written informed consent was obtained from all patients. From September 2010 to June 2014, 31 consecutive patients who were referred to our hospital to undergo a super-selective arterial infusion of cisplatin with concomitant radiotherapy under a diagnosis of nasal or sinonasal cancer were prospectively enrolled with the following inclusion criteria: (1) histopathological diagnosis of SCC, and (2) planning for a full course of curative treatment with 70-Gy radiation. In all patients, magnetic resonance imaging (MRI) including multiple b-value DWI for the acquisition of IVIM and DKI data was performed in both the pretreatment and early treatment periods.

Among these 31 patients, three discontinued treatment due to severe complications and were excluded. A total of 28 patients were thus eligible: 23 males (mean age 60.0 yrs, range 46–73 yrs) and five females (53.0 yrs, 43–59 yrs). The primary lesions involved the maxillary sinus in 25 patients and the nasal cavity in three patients. The histopathological diagnoses were SCC in all patients. The T stage was T2 in one patient, T3 in 11, T4a in 11, and T4b in five. The treatment regimen was a super-selective arterial infusion of cisplatin with concomitant radiotherapy for all

patients. Treatment details were as follows: an arterial infusion of cisplatin (100–120 mg/m² per week for 4 weeks) to the primary tumor’s dominant blood supply, using a microcatheter, with concurrent radiotherapy of a total of 70 Gy in 35 fractions [2]. MRI scans including IVIM and DKI were performed in all patients before treatment and again in the early treatment period. The time interval between the pretreatment MRI and the treatment start was 1–27 days (9.3±3.9 days). MR scanning in the early treatment period was performed upon the delivery of 16–20 Gy (mean 19.2 Gy) of the total 70 Gy, immediately after the second arterial infusion of cisplatin.

Clinical endpoint

In all patients, clinical and radiological follow-ups were performed after the treatment to determine the final diagnosis of the local control/failure at the primary site. Local failure was determined by the histopathological confirmation of SCC by biopsy or surgical resection, the development of a new mass in the post-treatment granulation tissue, or residual tumor enlargement during follow-up, which was ≥ 1 year (minimum follow-up period was set 1 year). Local control was determined by histopathological confirmation of the absence of SCC by surgical resection, absence of enlargement of the suspected lesion of the residual tumor, or absence of a new lesion in the post-treatment

granulation tissue within the follow-up period.

MR imaging protocol

All MR imaging was performed using a 3.0 Tesla unit (Achieva TX; Philips Healthcare, Best, Netherlands) with a 16-channel neurovascular coil. The DWI acquisition of IVIM and DKI data used single-shot spin-echo echo-planar imaging (EPI) with three orthogonal motion probing gradients. Twelve b-values (0, 10, 20, 30, 50, 80, 100, 200, 400, 800, 1000, and 2000 s/mm²) were used. The other imaging parameters were: TR, 4500 ms; TE, 64 ms; DELTA (large delta; gradient time interval), 30.1 ms; delta (small delta; gradient duration), 24.3 ms; flip angle, 90°; FOV, 230×230 mm; 64×64 matrix; slice thickness, 5 mm×20 slices; voxel size 3.59×3.59×5.00 mm; parallel imaging acceleration factor, 2; numbers of signal averages, b-value of 0–100 s/mm² (one average), 200–800 s/mm² (two averages) and 1000–2000 s/mm² (three averages); scanning time, 4 min 37 s.

Conventional MR images were also obtained to evaluate the primary tumor. These images included (a) axial T1-weighted image (T1WI) with a spin-echo sequence (TR, 450 ms; TE, 10 ms; FOV, 240×240 mm; 512×512 matrix; slice thickness, 5 mm; inter-slice gap, 30%; scanning time, 2 min 12 s), and (b) axial T2-weighted image

(T2WI) with a turbo spin-echo (TSE) sequence with fat suppression (TR, 4500 ms; TE, 70 ms; TSE factor, 9; FOV, 240×240 mm; 512×512 matrix; slice thickness, 5 mm; inter-slice gap, 30%; scanning time, 2 min 06 s).

Analysis of IVIM and DKI data

Using the signal intensity of all 12 b-values, we calculated the IVIM parameters perfusion fraction, f ; the pseudo-diffusion coefficient, D^* ; and the true diffusion coefficient, D . Using the signal intensity of five b-values (0, 400, 800, 1000 and 2000 s/mm^2), we calculated the DKI data. To obtain IVIM parameters, we applied the image signal intensity of each b-value to the following bi-exponential function [10]:

$$\frac{S_{(b)}}{S_0} = f \cdot e^{-b \cdot D^*} + (1 - f) \cdot e^{-b \cdot D} \quad [1]$$

To obtain DKI parameters (i.e., the kurtosis value, K and the kurtosis corrected diffusion coefficient, D_k), we applied the signal intensity data of five b-values (0, 400, 800, 1000 and 2000) using the following equation [22]:

$$\frac{S_{(b)}}{S_0} = \exp\left[-b * D_k + \frac{1}{6} * b^2 * D_k^2 * K\right] \quad [2]$$

where $S_{(b)}$ is the signal intensity at the b-value denoted by the subscript, S_0 is the signal intensity at the b-value of 0, and b is b-factor, in both Eqs. [1] and [2]. We fitted the signal intensity of b-values in Eqs. [1] and [2] with least square fitting using the Levenberg-Marquardt algorithm.

For the IVIM, we used a two-step fitting method for calculating the increase in the robustness of the fitting with less calculation error as follows: (1) the data of $b > 400 \text{ s/mm}^2$ were fitted for the single parameter D , because D^* is assumed to be significantly $> D$, so that the influence of pseudo-diffusion on signal decay can be neglected for b-values $> 400 \text{ s/mm}^2$. (2) The curve was fitted for f and D^* over all b-values, while keeping D constant [10, 23].

For the DKI, direct fitting to Eq. [2] was performed. The IVIM and DKI parameter calculations were performed on a pixel-by-pixel basis. Maps of f , D , D^* , K and D_k values were each obtained on a pixel-by-pixel basis from each pixel's signal intensity in the IVIM and DKI data.

The conventional ADC was also calculated using two b-values (0 and 1000). The following equation was used for the ADC calculation:

$$(\text{Signal intensity of } b=1000) / (\text{Signal intensity of } b=0) = \exp(-1000 * \text{ADC})$$

All parameter calculations were performed using MATLAB ver. 2012a (MathWorks, Natick, MA).

ROI delineation and parameter calculations

In the IVIM analysis, a board-certified neuroradiologist (A.T., 18 years' experience) delineated each tumor with a polygonal ROI on b0 images; axial T1WI and T2WI were used as reference images. Any area which was suggested to be a necrosis or cystic lesion was excluded from the ROI. If the tumor extended into two or more slices, all slices in which the tumor was included were used for the ROI delineation. Each delineated tumor ROI was copied on each parameter (f, D*, D, K, D_k and ADC) map. Each f, D*, D, K, D_k and ADC value was determined as the mean value in the delineated ROI by integrating all tumor voxels from all delineated slices into the total signal intensity.

For each pixel, the upper and lower limits were set for f and D* values to exclude unrealistic measurements (probably because of several outliers) to avoid including any erroneous pixels in the calculation. The lower and upper limits of f and D* were respectively set at 0–0.4 and 0–50×10⁻³ by referring to the range of each parameter in an earlier report (12). We performed a histogram analysis by calculating the 25th, 50th

and 75th percentile values of f , D^* , D , K , D_k and ADC in each tumor ROI. In addition, to assess the goodness of fit in both the IVIM and DKI fitting, we calculated the coefficient of determination (R^2 value; $R^2 = 1 - \text{ESS}/\text{TSS}$, where ESS is the sum of the squared errors between the data points and IVIM/DKI fitting curve, and TSS is the sum of the squared differences between the data points and the mean value of all data points) in each pixel [24]. When a pixel's R^2 value was < 0.8 , the pixel was excluded from the parameter calculation.

Statistical analysis

We used Pearson's correlation coefficient to assess the correlations of IVIM and DKI parameters (between the two sets of mean f , D^* , D , K , D_k and ADC values) at pretreatment, at the early treatment period and the percentage change between these two periods.

In a univariate analysis, the Mann-Whitney U-test was used to compare mean f , D^* , D , K , D_k and ADC values at the pretreatment, at the early-treatment period and the percentage change of these two periods between the local control and failure groups, respectively. The histogram (25th, 50th and 75th percentiles in the tumor) of these parameters (f , D^* , D , K , D_k and ADC) were also compared in the same trend. If a

significant difference was obtained for more than two parameters among the mean or histogram parameters, these parameters were analyzed by multivariate logistic regression models to determine whether they had independent predictive value with odds ratios (OR) and corresponding 95% confidence intervals (CI). The detected predictive values were also assessed using receiver operating characteristic (ROC) curves constructed for calculating the area under the curve (AUC). The diagnostic accuracy was determined by using the closest point to the upper left corner of the ROC curve in the division of local control and failure.

We conducted a univariate Cox regression analysis to predict aspects of the outcomes including the time point at which local failure was determined, adjusting each model separately for the parameters (f, D*, D, K, D_k, ADC at pretreatment, at the early treatment period, and the percentage change between these two periods), patient age and T stage (T2–3 vs. T4). If several significant parameters were detected regarding the relation to patient outcome, we conducted a multivariate analysis. Hazard ratios (HRs) and corresponding 95% CIs were calculated.

P-values <0.05 were considered significant. SPSS software (IBM, Armonk, NY) was used for all analyses.

RESULTS

We successfully obtained IVIM and kurtosis parameter maps for all 28 primary tumors in both the pretreatment and early treatment periods. Among the 28 patients, 9 patients were found to be local failure. Eight patients with local failure were confirmed by histopathological findings. One local failure and 19 local controls were determined by clinical diagnosis at follow-up (mean 23 mos; range 12–38 mos). All of the parameter data at the pretreatment, at the early treatment period and the percentage changes between these two periods are presented in Table 1. For each pixel within the tumor ROI, the coefficient of determination (R^2 value) was 0.94 ± 0.03 in the IVIM fitting and 0.97 ± 0.02 in the DKI fitting. Figure 1 presents a case example of all DW images, all parameter maps and the map of the R^2 values.

The Pearson's correlation coefficients between all parameters in the pretreatment period and during treatment and the percentage changes are summarized in Table 2.

The univariate analysis revealed significant differences between the local control and failure groups in pretreatment f values (mean, 25th, 50th, 75th percentiles), and the percentage change of D (mean, 25th, 50th, 75th), K values (mean, 50th, 75th), D_k values (mean, 25th, 50th, 75th), and ADCs (mean, 25th, 50th, 75th), respectively. The multivariate analysis revealed that the percentage change of D (mean, 25th, 50th, 75th

percentiles), K value (mean, 50th, 75th), Dk value (mean, 25th, 50th), and ADC (mean, 25th, 50th) were predictors for determining local control (Table 3). From the ROC curve analysis, the AUC, sensitivity, specificity, positive predictive value, negative predictive value, accuracy and cut-off value were calculated (Table 4). The parameter with the highest accuracy was the percentage change of D value with the histogram 25th percentile. Figure 2 presents a case example of D maps.

The univariate Cox regression analyses revealed the following significant predictors of treatment outcome: T-stage, the percentage change of D value (mean, 25th, 50th, 75th percentiles), K value (mean, 50th, 75th), Dk value (mean, 25th, 50th), and ADC (mean, 25th, 50th). The multivariate Cox regression analyses indicated that the predictors were the percentage change of D value (mean, 25th, 50th percentiles), K value (mean, 50th, 75th), Dk value (mean, 25th, 50th), and ADC (mean, 25th, 50th). The percentage change of D value with the histogram 25th percentile was also the highest HR. Table 5 summarizes these results.

DISCUSSION

Our findings revealed percentage change of several IVIM and DKI parameters between the pretreatment and the early treatment period as predictors of local control in

nasal or sinonasal SCC, while all absolute values of IVIM/DKI parameters at pretreatment and at the early treatment period were revealed non-significant. The IVIM parameter of D with the histogram 25th percentile was suggested to be the most powerful predictor.

In addition, a certain degree of correlations between several IVIM and DKI parameters was revealed. These IVIM and DKI parameters included the information of water diffusion, which reflects numerous tissue structures (e.g., the cellular compartment and the extracellular extravascular space), which indirectly affected the DWI signal in each b-value. Several parameters probably overlapped such tissue structural information, thus providing a significant correlation, although mainly reflected structure in each parameter may be different.

Being able to predict the local outcome of a primary tumor would provide useful information about the need for additional chemotherapy and possible earlier salvage surgery after the current chemoradiotherapy. Moreover, detecting parameter changes related to local control during treatment could help improve treatment planning. For example, radiotherapy is often re-planned due to a reduction in irradiated tumor volume after an interim evaluation. The local distribution of IVIM or DKI parameters percentage changes might be useful for re-planning radiotherapy, just as with FDG-PET

[25]. In arterial infusion therapy, the dose distribution of drug infusion in each artery can also be adjusted depending on the regional percentage change of IVIM or DKI parameters in each arterial territory [26]. If a poor outcome is strongly indicated, it may thus be possible to change the treatment plan (e.g., for a surgical resection) by interrupting the current treatment method.

The usefulness of the ADC for predicting patients' local outcomes has been described [6], but few reports discuss the usefulness of IVIM and DKI parameters for predicting treatment outcomes in head and neck lesions. There has apparently been no study assessing long-term treatment outcomes using both IVIM and DKI parameters in pretreatment and the early treatment period in SCC patients. Our present findings systematically revealed the overall usefulness of these parameters in nasal or sinonasal SCC patients.

Concerning IVIM parameters in head and neck lesions, Xiao et al. reported that the baseline D and early change of D were correlated with nasopharyngeal cancer patients' treatment response to neoadjuvant chemotherapy, although that series' histopathology was undifferentiated cancer in the nasopharynx [13], unlike the present study. Similar to the Xiao study, the percentage change of D was revealed herein as a significant predictor of local control, although the baseline D was not observed to be

significant. We speculate that the D value reflects more detail about intratumoral cell density and stromal space than the ADC because the calculation of D excludes the perfusion-related signal in the pixels, unlike the ADC calculation.

We suspect that another reason for the efficacy of the histogram 25th percentile of D is that it reflects the intratumoral heterogeneity for the sensitivity of treatment response in the whole tumor, e.g., a hypoxic lesion around the necrotic tissue, or a deep area of the tumor with lower perfusion [27, 28]. Such regions tend to be resistant to treatment and are more likely to be a residual tumor after treatment. These regions can be detected by the histogram analysis of the 25th percentile as a lower D-value area, while other regions of higher treatment sensitivity areas show increased D values. If the whole-tumor mean D value is used, such a focal area with treatment resistance is averaged with another region, resulting in a failure to detect such focal regions within a residual tumor.

This study also revealed significant correlations between the treatment outcome and the percentage change of K and D_k values at the early treatment period in both the logistic regression and Cox regression analyses. The associations between DKI parameters and the diagnosis of local control remain complex and unclear, but as also reported [29, 30], we suspect that K and D_k values reflect tissue microstructural

complexity (e.g., tumor cell density, stromal volume of the tumor tissue, and the complexity of the membrane structure) in more detail by a multiple b-value analysis with a non-linear fitting model. Therefore, the percentage change of DKI parameters might well reflect the microstructural-level damage of tumor tissue induced by the treatment, and may also reflect the treatment response in detail.

There is a technical issue related to the parameter calculation. We used all 12 b-values for the IVIM and five b-values for the DKI in the present study, but the series of b-value data varies among the prior and present studies, and the use of different b-value data might result in bias [31]. In the present study, D was calculated using the cutoff b-value of 400 mm/s^2 in reference to another IVIM report [23] to exclude perfusion-related signals as much as possible, whereas most of the other studies used $b=200 \text{ mm/s}^2$. Additionally, we set the highest b-value of 2000 mm/s^2 ; this was a slightly larger value than that used when targeting head and neck lesions. Such a high b-value signal will provide more details of restricted diffusion if a sufficient SNR is obtained. However, the data obtained in the present study may differ from IVIM or DKI values obtained in other studies. Careful interpretation is needed when comparing the obtained IVIM or DKI values — especially the absolute values.

This study has several limitations. First, the treatment method was the arterial infusion of cisplatin which have become popular in nasal or sinonasal SCC, but was not commonly used in cases of overall head and neck cancer; systemic therapy is frequently performed. Although we expect the reactivity in tumor-microenvironment by the chemoradiation used in the current study will not be much different from systemic chemoradiation or other non-surgical therapy, our findings should be carefully treated as reference data for other head and neck lesions. However, with this method, the early treatment period is easily set compared to systemic chemoradiation, the treatment regimen of which varies widely. Second, the number of patients (n=28) was not large, and we thus could not perform a subgroup analysis with divisions of histopathological differentiation or human papilloma virus status. However, nasal and sinonasal SCC are not very common, and it would be a challenge to investigate larger numbers of patients with nasal or sinonasal SCC. Third, we used a large pixel size for the acquisition of IVIM and DKI data; the reason for this was to obtain a high SNR in each pixel. All of the primary tumors in the present study included a large mass and were sufficient for the histogram analysis with such a large pixel size. However, a large pixel size could be inappropriate when small tumors are evaluated. In addition, the tumor ROI delineation was performed in b0 images in this study. We did not investigate which b-value image

was most appropriate to delineate the exact tumor ROI, and this remains to be determined in the future.

In conclusion, IVIM and DKI parameters — especially the IVIM D value with the histogram 25th percentile — were useful indicators for predicting treatment outcomes in nasal/sinonasal SCC patients. These parameters will contribute to decisions regarding treatment planning, additional treatment, and follow-up strategies, and thus to improved patient prognoses.

References

- 1 Wong SJ, Harari PM, Garden AS et al (2011) Longitudinal Oncology Registry of Head and Neck Carcinoma (LORHAN): analysis of chemoradiation treatment approaches in the United States. *Cancer* 117:1679-1686
- 2 Homma A, Sakashita T, Yoshida D et al (2013) Superselective intra-arterial cisplatin infusion and concomitant radiotherapy for maxillary sinus cancer. *Br J Cancer* 109:2980-2986
- 3 Homma A, Oridate N, Suzuki F et al (2009) Superselective high-dose cisplatin infusion with concomitant radiotherapy in patients with advanced cancer of the nasal cavity and paranasal sinuses: a single institution experience. *Cancer* 115:4705-4714
- 4 Eisenhauer EA, Therasse P, Bogaerts J et al (2009) New response evaluation criteria in solid tumours: revised RECIST guideline (version 1.1). *Eur J Cancer* 45:228-247
- 5 Cao Y, Popovtzer A, Li D et al (2008) Early prediction of outcome in advanced head-and-neck cancer based on tumor blood volume alterations during therapy: a prospective study. *Int J Radiat Oncol Biol Phys* 72:1287-1290

- 6 Srinivasan A, Mohan S, Mukherji SK (2012) Biologic imaging of head and neck cancer: the present and the future. *AJNR Am J Neuroradiol* 33:586-594
- 7 Kim S, Loevner L, Quon H et al (2009) Diffusion-weighted magnetic resonance imaging for predicting and detecting early response to chemoradiation therapy of squamous cell carcinomas of the head and neck. *Clin Cancer Res* 15:986-994
- 8 King AD, Chow KK, Yu KH et al (2013) Head and neck squamous cell carcinoma: diagnostic performance of diffusion-weighted MR imaging for the prediction of treatment response. *Radiology* 266:531-538
- 9 Hauser T, Essig M, Jensen A et al (2013) Characterization and therapy monitoring of head and neck carcinomas using diffusion-imaging-based intravoxel incoherent motion parameters—preliminary results. *Neuroradiology* 55:527-536
- 10 Fujima N, Yoshida D, Sakashita T et al (2014) Intravoxel incoherent motion diffusion-weighted imaging in head and neck squamous cell carcinoma: assessment of perfusion-related parameters compared to dynamic contrast-enhanced MRI. *Magn Reson Imaging* 32:1206-1213
- 11 Ding Y, Fuller C, Mohamed A, Wang J, Hazle J (2015) TU-F-CAMPUS-I-01: Head and neck squamous cell carcinoma: short-term repeatability of apparent

- diffusion coefficient and intravoxel incoherent motion parameters at 3.0T. *Med Phys* 42:3646
- 12 Marzi S, Piludu F, Vidiri A (2013) Assessment of diffusion parameters by intravoxel incoherent motion MRI in head and neck squamous cell carcinoma. *NMR Biomed* 26:1806-1814
- 13 Xiao Y, Pan J, Chen Y, He Z, Zheng X (2015) Intravoxel incoherent motion-magnetic resonance imaging as an early predictor of treatment response to neoadjuvant chemotherapy in locoregionally advanced nasopharyngeal carcinoma. *medicine (Baltimore)* 94:e973
- 14 Chen Y, Ren W, Zheng D et al (2015) Diffusion kurtosis imaging predicts neoadjuvant chemotherapy responses within 4 days in advanced nasopharyngeal carcinoma patients. *J Magn Reson Imaging*. 10.1002/jmri.24910
- 15 Lai V, Lee VH, Lam KO, Sze HC, Chan Q, Khong PL (2015) Intravoxel water diffusion heterogeneity MR imaging of nasopharyngeal carcinoma using stretched exponential diffusion model. *Eur Radiol* 25:1708-1713
- 16 Jia QJ, Zhang SX, Chen WB et al (2014) Initial experience of correlating parameters of intravoxel incoherent motion and dynamic contrast-enhanced magnetic resonance imaging at 3.0 T in nasopharyngeal carcinoma. *Eur Radiol*

24:3076-3087

- 17 Zhang SX, Jia QJ, Zhang ZP et al (2014) Intravoxel incoherent motion MRI: emerging applications for nasopharyngeal carcinoma at the primary site. *Eur Radiol* 24:1998-2004
- 18 Lai V, Li X, Lee VH et al (2014) Nasopharyngeal carcinoma: comparison of diffusion and perfusion characteristics between different tumour stages using intravoxel incoherent motion MR imaging. *Eur Radiol* 24:176-183
- 19 Wang LL, Lin J, Liu K et al (2014) Intravoxel incoherent motion diffusion-weighted MR imaging in differentiation of lung cancer from obstructive lung consolidation: comparison and correlation with pharmacokinetic analysis from dynamic contrast-enhanced MR imaging. *Eur Radiol* 24:1914-1922
- 20 Le Bihan D, Breton E, Lallemand D, Aubin ML, Vignaud J, Laval-Jeantet M (1988) Separation of diffusion and perfusion in intravoxel incoherent motion MR imaging. *Radiology* 168:497-505
- 21 Jensen JH, Helpert JA, Ramani A, Lu H, Kaczynski K (2005) Diffusional kurtosis imaging: the quantification of non-gaussian water diffusion by means of magnetic resonance imaging. *Magn Reson Med* 53:1432-1440

- 22 Rosenkrantz AB, Padhani AR, Chenevert TL et al (2015) Body diffusion kurtosis imaging: Basic principles, applications, and considerations for clinical practice. *J Magn Reson Imaging*. 10.1002/jmri.24985
- 23 Wu WC, Chen YF, Tseng HM, Yang SC, My PC (2015) Caveat of measuring perfusion indexes using intravoxel incoherent motion magnetic resonance imaging in the human brain. *Eur Radiol* 25:2485-2492
- 24 Suo S, Lin N, Wang H et al (2015) Intravoxel incoherent motion diffusion-weighted MR imaging of breast cancer at 3.0 tesla: Comparison of different curve-fitting methods. *J Magn Reson Imaging* 42:362-370
- 25 Delouya G, Igidbashian L, Houle A et al (2011) (1)(8)F-FDG-PET imaging in radiotherapy tumor volume delineation in treatment of head and neck cancer. *Radiother Oncol* 101:362-368
- 26 Fujima N, Yoshida D, Sakashita T et al (2015) Usefulness of pseudocontinuous arterial spin-labeling for the assessment of patients with head and neck squamous cell carcinoma by measuring tumor blood flow in the pretreatment and early treatment period. *AJNR Am J Neuroradiol*. 10.3174/ajnr.A4513
- 27 Evans SM, Du KL, Chalian AA et al (2007) Patterns and levels of hypoxia in head and neck squamous cell carcinomas and their relationship to patient

- outcome. *Int J Radiat Oncol Biol Phys* 69:1024-1031
- 28 Fujima N, Kudo K, Yoshida D et al (2014) Arterial spin labeling to determine tumor viability in head and neck cancer before and after treatment. *J Magn Reson Imaging* 40:920-928
- 29 Rosenkrantz AB, Sigmund EE, Johnson G et al (2012) Prostate cancer: feasibility and preliminary experience of a diffusional kurtosis model for detection and assessment of aggressiveness of peripheral zone cancer. *Radiology* 264:126-135
- 30 Sun K, Chen X, Chai W et al (2015) Breast cancer: diffusion kurtosis mr imaging-diagnostic accuracy and correlation with clinical-pathologic factors. *Radiology*. 10.1148/radiol.15141625:141625
- 31 Yuan J, Yeung DK, Mok GS et al (2014) Non-Gaussian analysis of diffusion weighted imaging in head and neck at 3T: a pilot study in patients with nasopharyngeal carcinoma. *PLoS One* 9:e87024

Figure and table captions

Fig. 1. DW images in each b-value, tumor ROI delineation, IVIM and DKI parameter maps and residual sum/R2 map in patients with right maxillary cancer. The original images of all b-values (0–2000) are presented (a) with the same window level/width in the range of 0-400 of b-value, whereas the window level/width was each adjusted for well visualization of the tumor in upper 800 of b-value. Each tumor was delineated with a polygonal ROI on b0 images in the raw images of IVIM (b). Axial T2WI (c) and T1WI (d) were used as reference images for the delineation. Each delineated tumor ROI was copied on each parameter's (f, D^* , D , K , D_k and ADC) map (e). R^2 maps of IVIM (f) and DKI (g) in the tumor ROI were presented for the assessment of goodness of fit.

Fig. 2. Patient with right maxillary SCC in pretreatment (a: T2WI, b: D map), early treatment period (c: T2WI, d: D map) and follow-up scanning after treatment (e: T2WI). Compared to the pretreatment T2WI (a: white arrows), it was difficult to discern a marked difference in T2WI at the early treatment period (c: white arrows). In the D map at the early treatment period (b: white arrows), an increase in the D values for most of the tumor was observed (d: white arrows); however, only a slight change in the D value

on the left-dorsal area in the tumor was observed (d: black arrow). This area was finally revealed as a residual tumor by follow-up T2WI after the treatment as development of mass lesion (e: white arrows) and histopathological findings. Such focal change was detected by the histogram analysis of the 25th percentile in the D map.

Table 1. All IVIM and DKI Parameters in the Pretreatment and Early Treatment Periods and the Percentage Change between the Two Periods

Table 1 footnote: Data are mean \pm standard deviation. D: true diffusion coefficient ($\times 10^{-3}$ mm²/s), f: perfusion fraction ($\times 10^2$ %), D*: fast diffusion coefficient ($\times 10^{-3}$ mm²/s), ADC: apparent diffusion coefficient ($\times 10^{-3}$ mm²/s), K: kurtosis value (dimensionless), D_k: kurtosis corrected diffusion coefficient ($\times 10^{-3}$ mm²/s), 25: 25th percentile value, 50: 50th percentile value, 75: 75th percentile value.

Table 2. The Pearson's Correlation Coefficients between the Two Sets of Mean f, D*, D, K, D_k and ADC in the Pretreatment and Early Treatment Periods and the Percentage Change

Table 2 footnote: *p<0.05. D: true diffusion coefficient, f: perfusion fraction, D*: fast diffusion coefficient, ADC: apparent diffusion coefficient, K: kurtosis value, D_k: kurtosis corrected diffusion coefficient.

Table 3. Significant Parameters in the Multivariate Logistic Regression Models

Table 3 footnote: Data are odds ratios and p-values. Data in parentheses are 95% confidence intervals. D: true diffusion coefficient, ADC: apparent diffusion coefficient,

K: kurtois value, D_k : kurtosis corrected diffusion coefficient.

Table 4. ROC Analysis Results

Table 4 footnote: AUC: area under curve, PPV: positive predictive value, NPV: negative predictive value, D: true diffusion coefficient, ADC: apparent diffusion coefficient, K: kurtois value, D_k : kurtosis corrected diffusion coefficient.

Table 5. Significant Parameters in the Cox-Proportional Hazards Regression Models

Table 5 footnote: Data are odds ratios and p-values. Data in parentheses are 95% confidence intervals. D: true diffusion coefficient, ADC: apparent diffusion coefficient, K: kurtois value, D_k : kurtosis corrected diffusion coefficient.

Figure1a

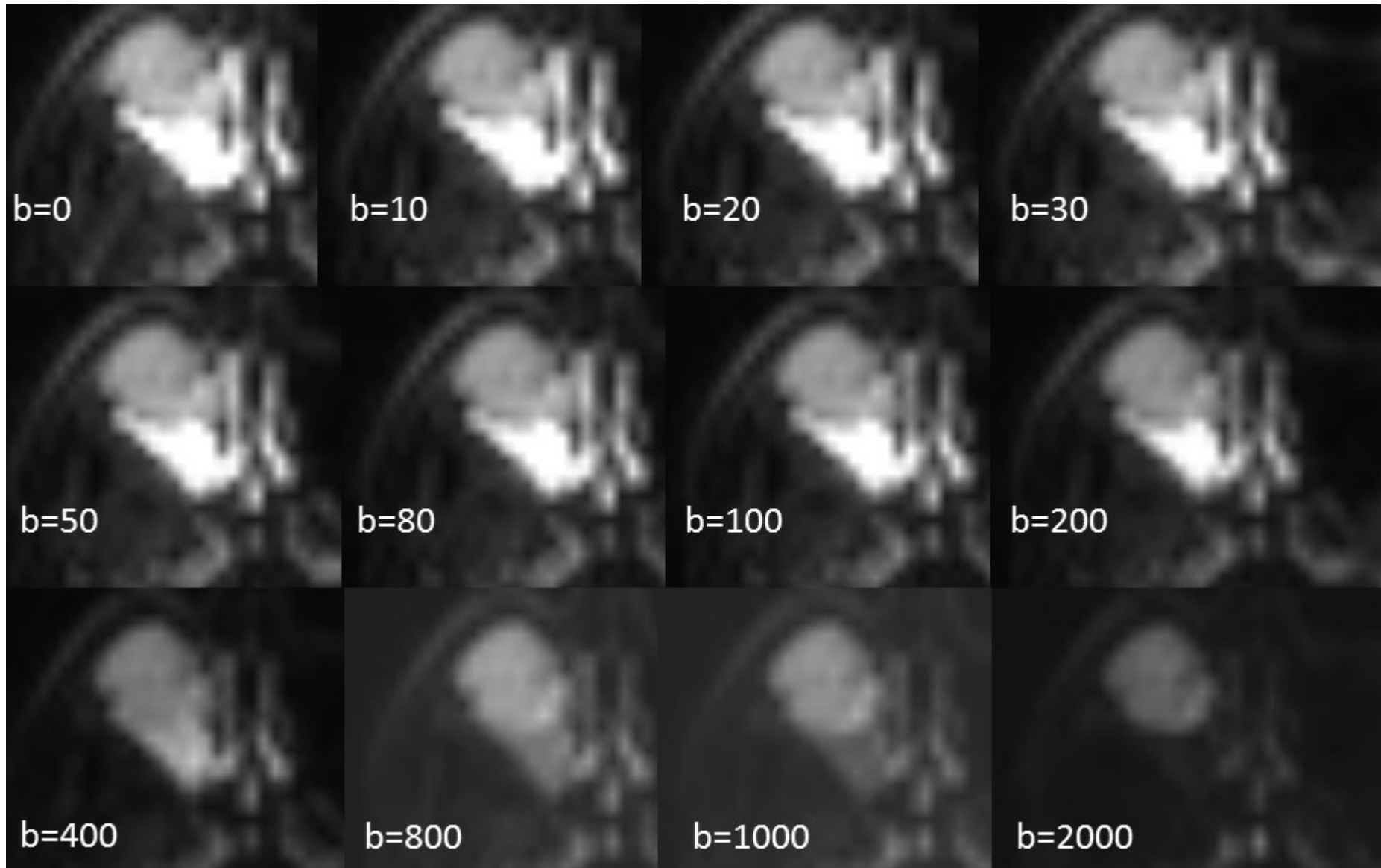


Figure1b

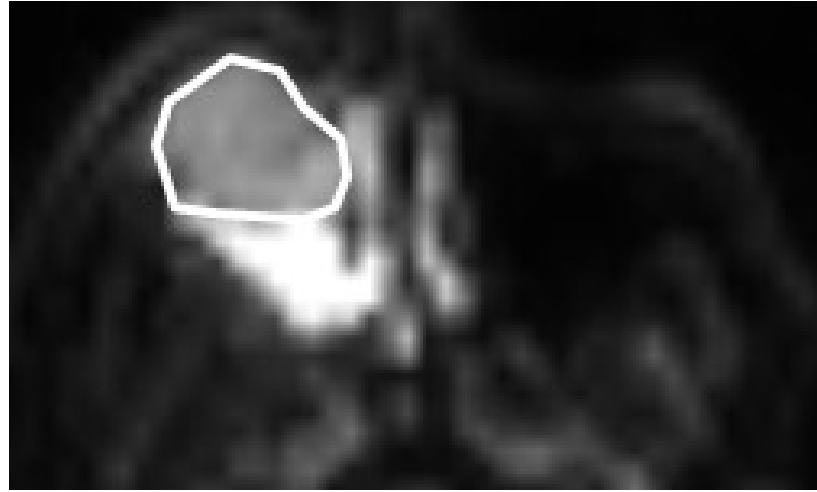


Figure1c



Figure1d

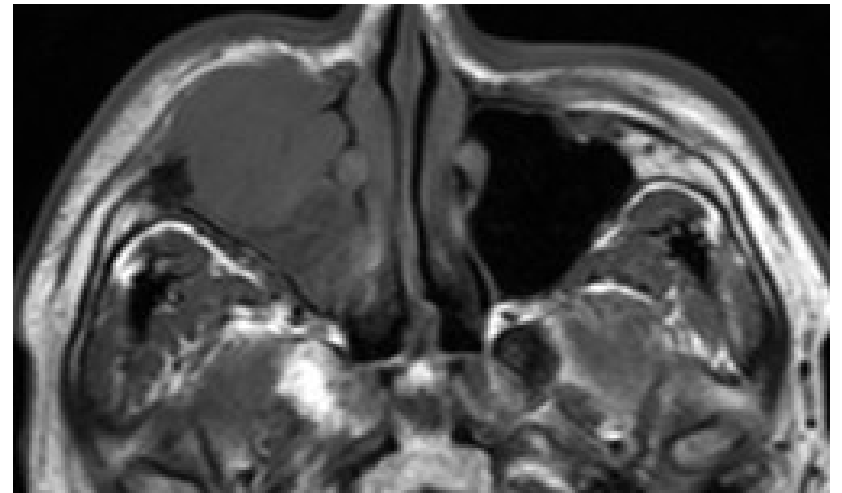


Figure1e

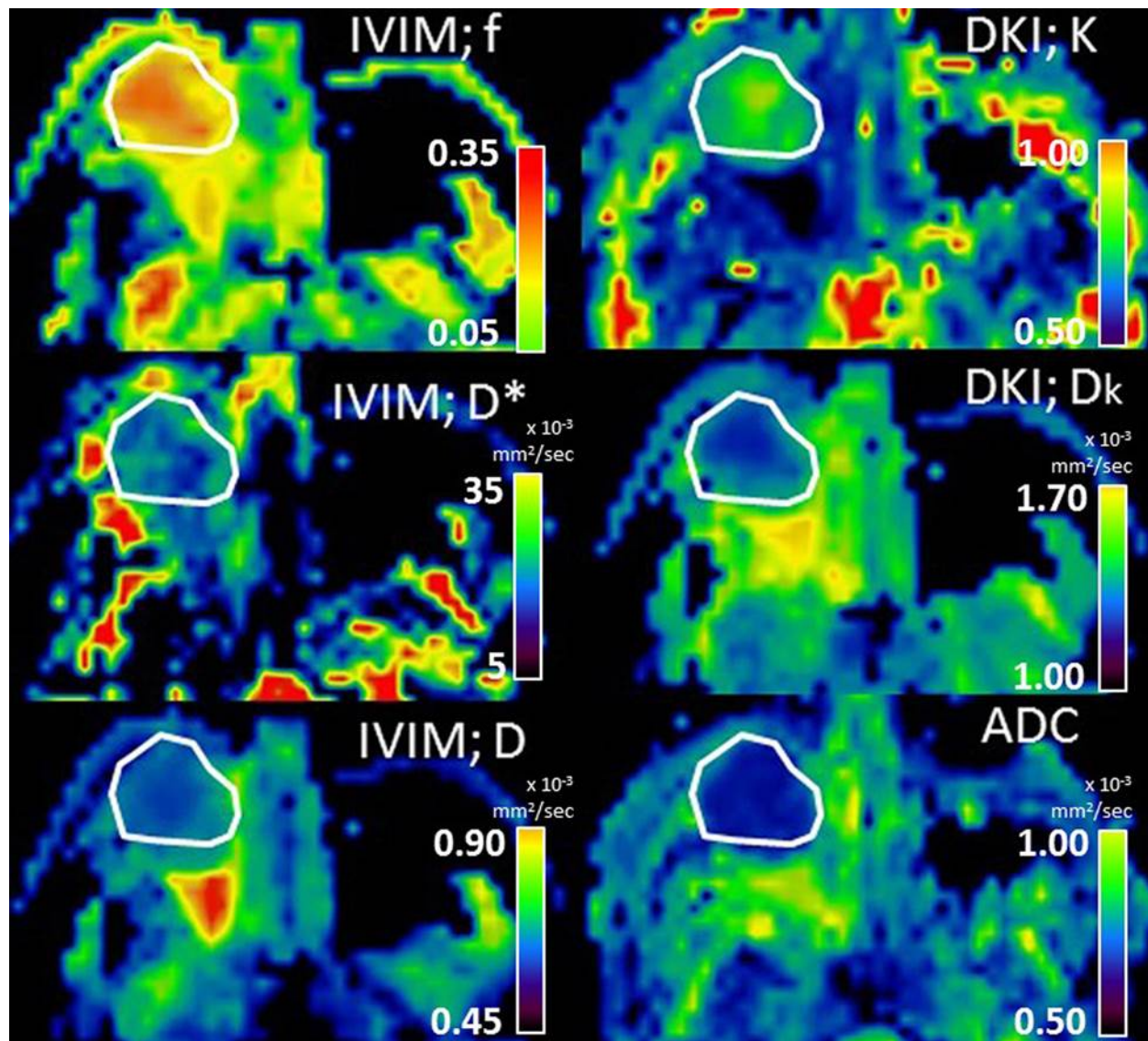


Figure1f

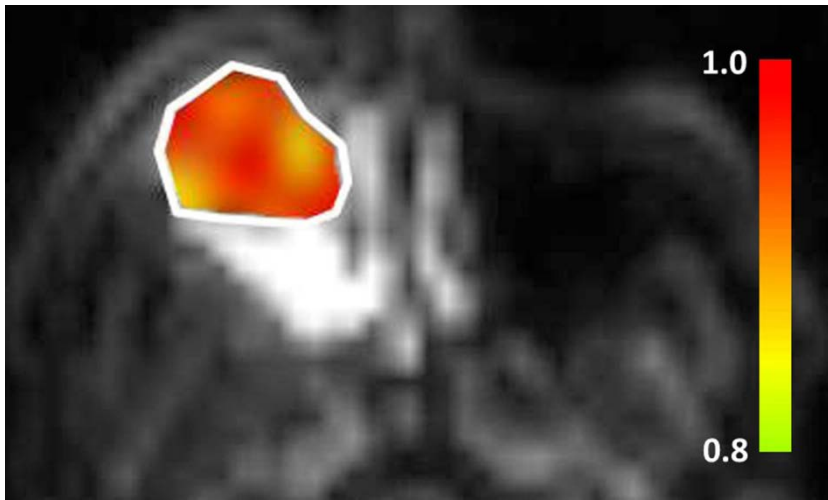


Figure1g

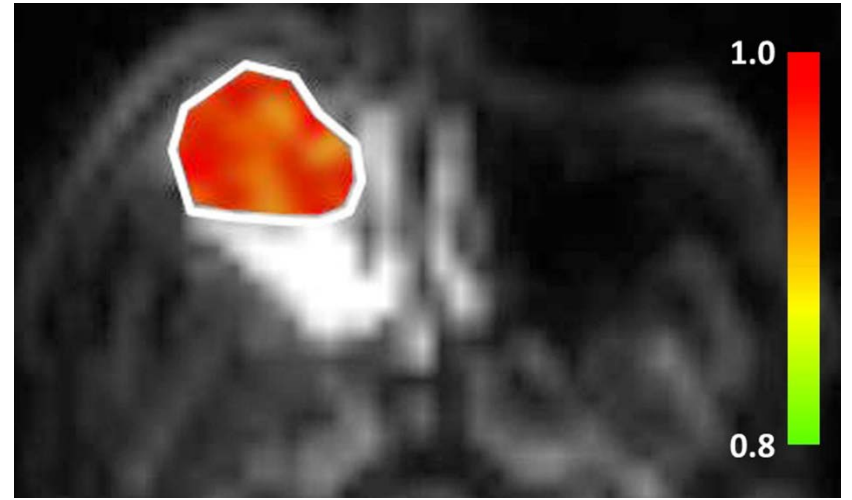


Figure2a

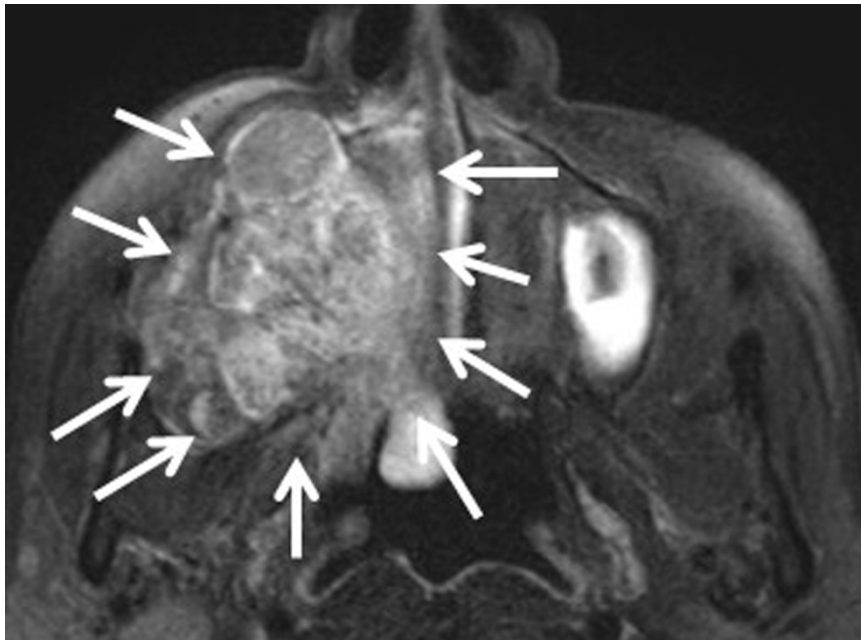


Figure2b

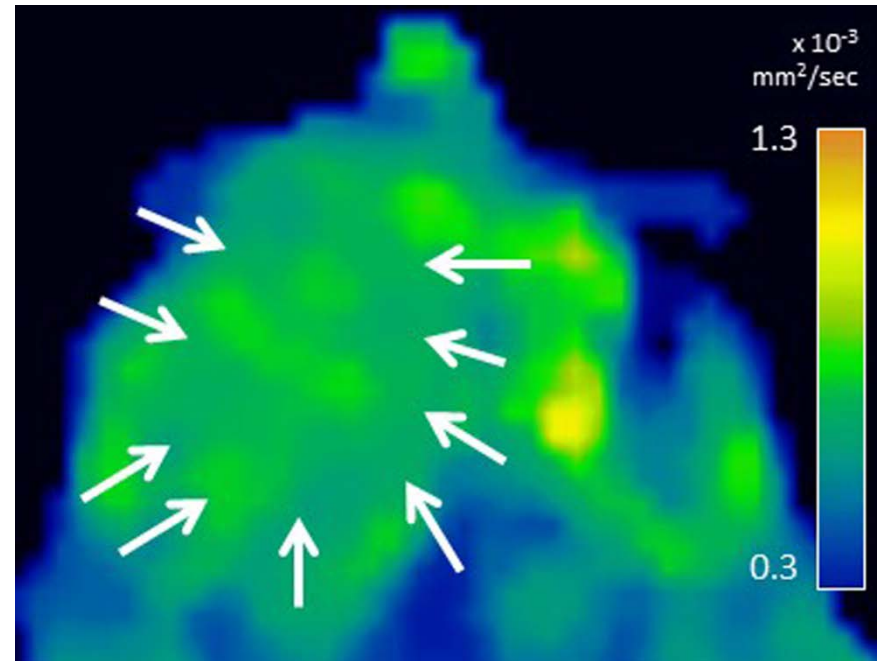


Figure2c

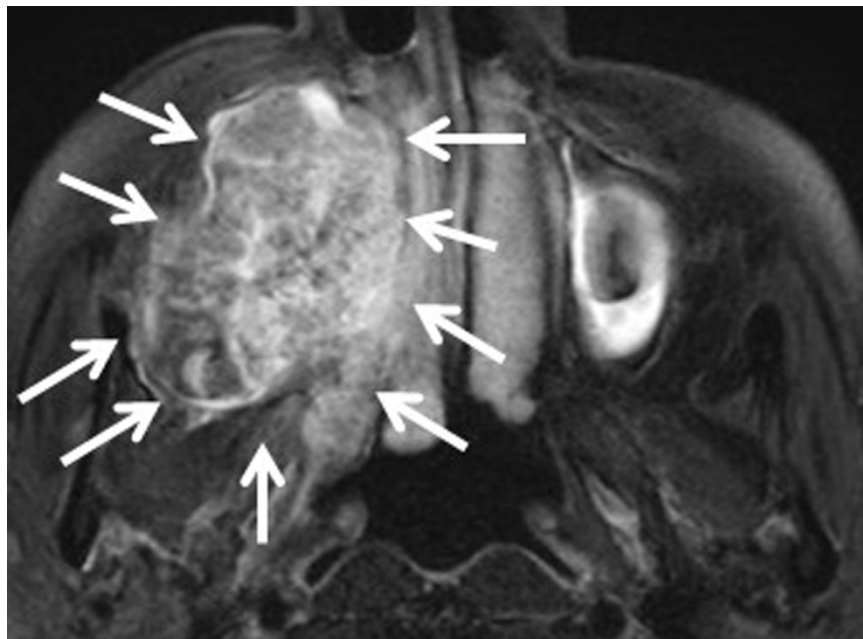


Figure2d

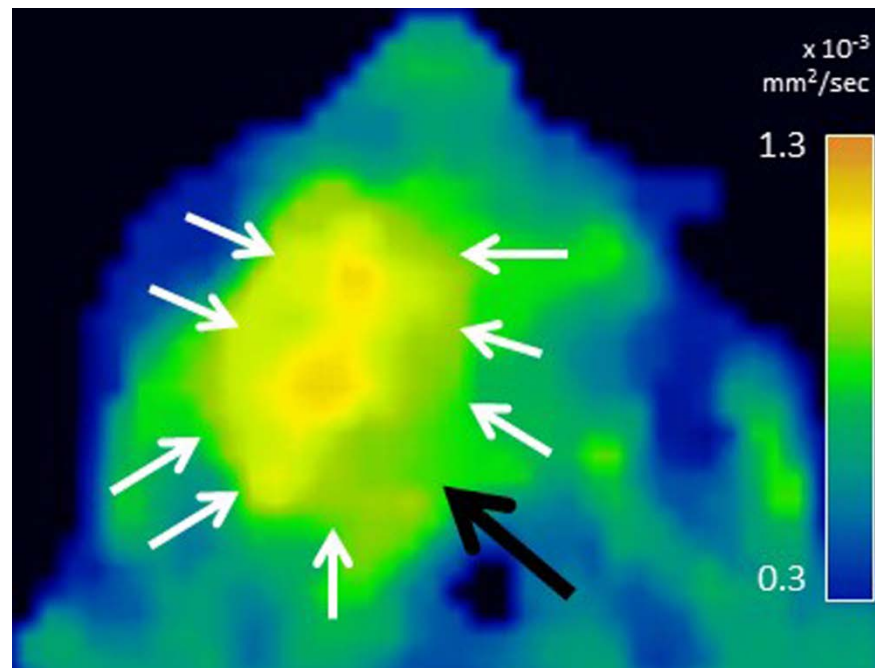


Figure 2e

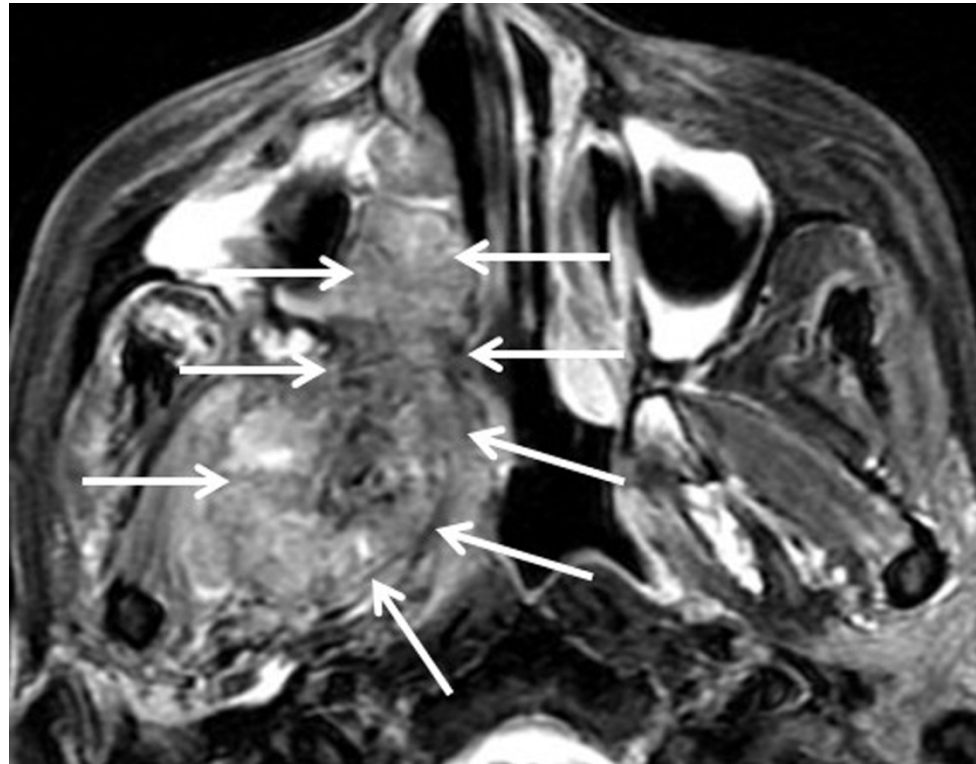


Table 1. All IVIM and DKI Parameters in the Pretreatment and Early Treatment Periods and the Percentage Change between the Two Periods.

		Pre-treatment		During treatment		Percentage change	
		Local control	Local failure	Local control	Local failure	Local control	Local failure
D	mean	0.72±0.07	0.70±0.05	0.94±0.15	0.81±0.08	30.1±15.0	16.1±6.7
	25	0.66±0.06	0.65±0.04	0.85±0.15	0.73±0.08	28.9±12.5	11.5±6.0
	50	0.73±0.08	0.71±0.05	0.96±0.16	0.82±0.09	31.3±15.4	16.2±7.4
	75	0.78±0.08	0.76±0.06	1.05±0.19	0.88±0.16	33.6±16.8	19.5±12.0
f	mean	0.19±0.04	0.14±0.03	0.19±0.11	0.14±0.08	0.7±20.2	-2.6±5.9
	25	0.14±0.03	0.11±0.02	0.15±0.08	0.12±0.07	7.7±15.7	3.5±6.7
	50	0.18±0.04	0.14±0.03	0.20±0.10	0.16±0.08	6.9±16.0	5.7±5.9
	75	0.22±0.05	0.19±0.04	0.24±0.12	0.19±0.09	7.9±17.1	4.2±5.9
D*	mean	30.1±7.4	27.0±7.1	31.3±8.2	27.4±8.3	4.9±21.4	2.1±16.2
	25	23.1±6.1	19.9±5.2	26.46±6.9	20.0±7.6	12.9±19.8	6.1±23.7
	50	29.7±7.0	26.5±6.6	31.5±8.3	26.9±8.4	12.4±16.7	5.1±14.2
	75	34.3±8.9	33.4±8.8	37.8±9.1	34.3±10.4	10.2±16.4	6.2±20.4
ADC	mean	0.83±0.09	0.81±0.06	1.08±0.17	0.94±0.09	29.8±13.5	18.8±8.5
	25	0.75±0.08	0.76±0.05	0.96±0.14	0.87±0.07	28.4±11.7	16.9±7.1
	50	0.82±0.10	0.81±0.06	1.01±0.17	0.94±0.09	32.0±14.4	17.0±8.1
	75	0.90±0.11	0.87±0.06	1.20±0.20	1.02±0.11	32.7±18.2	19.9±10.5
K	mean	0.81±0.09	0.80±0.06	0.61±0.11	0.71±0.09	-23.4±12.8	-10.8±5.9
	25	0.73±0.07	0.75±0.06	0.57±0.10	0.63±0.08	-24.0±13.0	-17.0±5.5
	50	0.80±0.08	0.81±0.07	0.60±0.11	0.71±0.08	-23.5±13.6	-11.7±4.9
	75	0.86±0.10	0.84±0.08	0.66±0.12	0.75±0.10	-22.7±14.4	-9.6±5.0
Dk	mean	1.37±0.19	1.31±0.17	1.91±0.19	1.63±0.23	45.1±22.6	24.5±14.3
	25	1.19±0.17	1.15±0.16	1.68±0.16	1.45±0.18	48.0±22.8	19.8±12.3
	50	1.38±0.18	1.31±0.18	1.91±0.18	1.63±0.22	44.9±21.8	24.3±13.0
	75	1.56±0.20	1.46±0.19	2.14±0.22	1.89±0.27	41.3±21.3	30.7±14.5

Table 1 footnote: Data are mean ± standard deviation. D: true diffusion coefficient

($\times 10^{-3}$ mm²/s), f: perfusion fraction ($\times 10^2$ %), D*: fast diffusion coefficient ($\times 10^{-3}$ mm²/s), ADC: apparent diffusion coefficient ($\times 10^{-3}$ mm²/s), K: kurtosis value (dimensionless), D_k: kurtosis corrected diffusion coefficient ($\times 10^{-3}$ mm²/s), 25: 25th percentile value, 50: 50th percentile value, 75: 75th percentile value.

Table 2. The Pearson's Correlation Coefficients between the Two Sets of Mean f, D*, D, K, D_k and ADC in the Pretreatment and Early Treatment Periods and the Percentage Change

Correlation between pretreatment values						
	D	f	D*	ADC	K	Dk
D	–	0.34	0.35	0.66*	–0.59	0.61*
f	–	–	0.29	0.13	–0.38	0.31
D*	–	–	–	0.23	–0.36	0.22
ADC	–	–	–	–	–0.52	0.61*
K	–	–	–	–	–	–0.44
Dk	–	–	–	–	–	–
Correlation between values during treatment						
	D	f	D*	ADC	K	Dk
D	–	0.49	0.09	0.77*	–0.37	0.69*
f	–	–	0.13	0.39	–0.03	0.31
D*	–	–	–	0.15	0.02	0.03
ADC	–	–	–	–	–0.33	0.72*
K	–	–	–	–	–	–0.34
Dk	–	–	–	–	–	–
Correlation between percentage changes						
	D	f	D*	ADC	K	Dk
D	–	0.23	0.13	0.71*	–0.16	0.42
f	–	–	0.46	0.32	0.22	0.23
D*	–	–	–	0.23	0.1	0.07
ADC	–	–	–	–	–0.03	0.56
K	–	–	–	–	–	–0.23
Dk	–	–	–	–	–	–

Table 2 footnote: *p<0.05. D: true diffusion coefficient, f: perfusion fraction, D*: fast

diffusion coefficient, ADC: apparent diffusion coefficient, K: kurtosis value, D_k :
kurtosis corrected diffusion coefficient.

Table 3. Significant Parameters in the Multivariate Logistic Regression Models

Significant Parameters in Multivariate Logistic Regression Models

Parameter	Odds ratio	P value
<hr/>		
Percentage change during treatment		
<hr/>		
D, mean	7.1 (1.9, 35.6)	0.002
D, 25 percentile	12.4 (2.7, 74.4)	<0.001
D, 50 percentile	6.1 (1.5, 29.5)	0.006
D, 75 percentile	5.7 (1.2, 25.7)	0.007
ADC, mean	2.9 (0.9, 6.2)	0.013
ADC, 25 percentile	6.1 (1.3, 27.9)	0.007
ADC, 50 percentile	2.7 (1.1, 5.3)	0.025
K, mean	5.9 (1.3, 28.1)	0.006
K, 50 percentile	4.9 (0.9, 12.5)	0.009
K, 75 percentile	6.4 (1.4, 35.7)	0.007
D _k , mean	4.6 (1.3, 13.9)	0.008
D _k , 25 percentile	5.5 (1.2, 23.4)	0.008
D _k , 50 percentile	4.2 (0.8, 12.1)	0.017

Table 3 footnote: Data are odds ratios and p-values. Data in parentheses are 95%

confidence intervals. D: true diffusion coefficient, ADC: apparent diffusion coefficient,

K: kurtosis value, D_k: kurtosis corrected diffusion coefficient.

Table 4. ROC Analysis Results

The Results of ROC analysis

Parameter	AUC	Sensitivity	Specificity	PPV	NPV	Accuracy	Cut off value
Percentage change during treatment							
D, mean	0.84	0.89	0.67	0.85	0.75	0.82	17.4
D, 25th percentile	0.96	0.89	1	1	0.82	0.93	17.8
D, 50th percentile	0.8	0.89	0.67	0.85	0.75	0.82	17.2
D, 75th percentile	0.74	0.84	0.67	0.84	0.67	0.79	16.5
ADC, mean	0.75	0.84	0.56	0.8	0.63	0.75	11.9
ADC, 25th percentile	0.8	0.89	0.67	0.85	0.75	0.82	12.1
ADC, 50th percentile	0.76	0.84	0.67	0.67	0.67	0.79	12
K, mean	0.81	0.68	0.89	0.93	0.57	0.75	-15
K, 50th percentile	0.79	0.74	0.89	0.93	0.62	0.79	-11.9
K, 75th percentile	0.82	0.79	0.89	0.94	0.67	0.79	-13.3
D _k , mean	0.76	0.79	0.78	0.88	0.64	0.78	30.3
D _k , 25th percentile	0.78	0.79	0.89	0.94	0.67	0.82	31
D _k , 50th percentile	0.78	0.79	0.78	0.88	0.64	0.79	29.1

Table 4 footnote: AUC: area under curve, PPV: positive predictive value, NPV: negative predictive value. D: true diffusion coefficient, ADC: apparent diffusion coefficient, K: kurtois value, D_k: kurtosis corrected diffusion coefficient.

Table 5. Significant Parameters in the Cox-Proportional Hazards Regression Models

Significant Parameters in Cox-Proportional Hazards Regression Models

Parameter	Hazard ratio	P value
<hr/>		
Percentage change during treatment		
<hr/>		
D, mean	5.9 (1.1, 25.1)	0.01
D, 25 percentile	7.1 (1.4, 41.5)	0.002
D, 50 percentile	5.6 (0.7, 28.8)	0.016
ADC, mean	2.3 (0.8, 4.3)	0.29
ADC, 25 percentile	2.5 (0.9, 4.7)	0.35
ADC, 50 percentile	2.1 (0.7, 3.9)	0.29
K, mean	3.2 (1.0, 7.8)	0.01
K, 50 percentile	3.1 (0.9, 6.1)	0.015
K, 75 percentile	4.1 (1.2, 13.7)	0.009
D _k , mean	2.8 (1.1, 5.0)	0.031
D _k , 25 percentile	3.1 (1.2, 6.2)	0.022
D _k , 50 percentile	1.9 (1.0, 3.5)	0.035

Table 5 footnote: Data are odds ratios and p-values. Data in parentheses are 95% confidence intervals. D: true diffusion coefficient, ADC: apparent diffusion coefficient, K: kurtosis value, D_k: kurtosis corrected diffusion coefficient.